Electronic Supplementary Material (ESI) for Chemical Science.
This journal is © The Royal Society of Chemistry 2019

Supporting Information

Engineering High Reversibility and Fast Kinetics of Bi Nanoflakes by Surface Modulation for Ultrastable Nickel-Bismuth Batteries

Yinxiang Zeng,[a] Mengying Wang,[a] Wanyi He,[a] Pingping Fang,[a] Mingmei Wu,*[a] Yexiang Tong,[a] Minghua Chen,*[b] and Xihong Lu*[a,b]

a. MOE of the Key Laboratory of Bioinorganic and Synthetic Chemistry, KLGHEI of Environment and Energy Chemistry, School of Chemistry, Sun Yat-Sen University, Guangzhou 510275, China, E-mail: luxh6@mail.sysu.edu.cn; ceswmm@mail.sysu.edu.cn
b. Key Laboratory of Engineering Dielectric and Applications (Ministry of Education), Harbin University of Science and Technology, Harbin 150080, China

Experimental details

Synthesis of Bi and BiO_x sample on carbon cloth: Bi was prepared by electrodeposition at -0.8 V for 20 min at room temperature. The electrolyte for electrodeposition was a mixed solution by dissolving 1 mmol $Bi(NO_3)_3 \cdot 5H_2O$, 4 mmol ETDA and 1 mmol hexadecyltrimethylammonium bromide (CTMAB) into 20 mL distilled water. After electrodeposition, the obtained sample was washed with distilled water and dried in a vacuum oven at 60 °C. To realize the surface oxidation of Bi (BiO_x), the as-prepared Bi sample was further undergoing controllable successive water oxidation process by atomic layer deposition (ALD) technology (ALD-SC6-PE, Syskey Technology Co., Ltd.). Additionally, the as-prepared Bi sample was also calcined at 200 °C for 5 min in air to complete the surface oxidation of Bi.

Synthesis of Ni-NiO on carbon cloth: Ni-NiO was prepared by electrodeposition of Ni and followed by oxidation. The electrodeposition of Ni was conducted at -1.4 V for 15 min at room temperature. Electrolyte for electrodeposition (20 mL) contain 5 mmol $Ni(NO_3)_2 \cdot 6H_2O$, 5 mmol $NiCl_2$, 25 mmol H_3BO_3 and 1.735 mmol sodium lauryl sulfate. After electrodeposition, the as-prepared sample was washed with distilled water and then oxidized by sonicating in the solution containing 35 mL 4 M HCl and 15 mL ethanol for 5 min. The as-obtained sample was placed under ambient conditions for 15 min to derive Ni-NiO electrode at room temperature.

Structural Characterization*:* the microstructures and compositions of the electrode materials were analyzed using field-emission SEM (FE-SEM, JSM-6330F), transmission electron microscopy (TEM, FEI Tecnai G2 F30), Raman spectroscopy (Renishaw inVia), and X-ray diffractometry (XRD, D8 ADVANCE). XPS was carried out at BL10B and BL12B beamlines in NSRL, Hefei. Thermogravimetric analysis (TGA) curves were conducted by using a Netzsch TG209F1 analyzer. The thickness and the morphology of the BiO_x nanoflakes were measured in air using Digital Instrument Shimadzu AFM (SPM-9500J3) with a silicon microcantilever (spring constant of 30 N m^{-1} and resonance frequency of ~270 kHz). The ultrasounding was carried out using a Shumei ultrasound cleaner (KQ-400DE) with power of 400 W and frequency of 40 kHz. The *in situ* Raman test was run on a laser micro-Raman spectrometer (Renishaw inVia) equipped with a He-Ne laser (wavelength = 514.5 nm) and a long working distance 50× objective lens. Raman spectra of the sample were captured with exploration time of 30 s after certain cycles of CV test in a three electrode cell at a scan rate of 100 mV s^{-1}.

Electrochemical Measurement*:* cyclic voltammetry (CV), galvanostatic charge/discharge measurements and electrochemical impedance spectroscopy were conducted employing an electrochemical workstation (CHI 760E). The electrochemical studies of the individual electrode were performed in a three-electrode cell, with a carbon rod auxiliary electrode and a saturated calomel electrode (SCE) reference electrode. All the electrochemical characterizations for electrodes and aqueous Ni//Bi battery were performed in 1 M KOH aqueous solution.

Calculations:

1. Single Electrode :

The areal capacities of the Bi、BiO_x and NiO electrodes were measured by galvanostatic charge/discharge method based on the following equation:

$$C_s = \frac{\int_0^{\Delta t} I \times dt}{S} \quad (1)$$

where C_a (mA h cm^{-2}) is the areal capacity, I (mA) is the constant discharging current, Δt (h) is the discharging time and S (cm^2) is the area of electrode.

2. Ni//Bi battery:

The areal capacities of the Ni//Bi battery ($C_{cell\text{-}a}$) were measured by galvanostatic charge/discharge method based on the following equation:

$$C_{cell-a} = \frac{\int_0^{\Delta t} I \times dt}{S} \quad (2)$$

where $C_{cell\text{-}s}$ (mA h cm^{-2}) is the areal capacity of the of the Ni//Bi battery, I (mA) is the constant discharging current, Δt (h) is the discharging time and S (cm^2) is the area of the Ni//Bi battery.

The energy density E and specific power density P of the Ni//Bi battery were obtained from the following equations:

$$E = \frac{\int_{V_1}^{V_2} C_{cell} \times dV}{d} \quad (3)$$

$$P = \frac{E}{1000 \times \Delta t} \quad (4)$$

where E (mWh cm^{-3}) is the energy density of the Ni//Bi battery, C_{cell} is the specific areal capacity obtained from Equation (4), V (V) is the voltage window and d is the thickness of the Ni//Bi battery (0.08 cm). P (W cm^{-3}) is the specific power density of the Ni//Bi battery and Δt (h) is the discharging time.

DFT Calculations:

All the calculations were performed based on density functional theory (DFT) implemented in The Vienna Ab-initio Software Package (VASP). The generalized

gradient approximation (GGA) in the scheme of Perdew-Burke-Ernzerhof (PBE) function was used to calculate the electron exchange-correlation interactions. All atomic positions and lattice vectors were fully optimized using a conjugate gradient algorithm to obtain the unstrained configuration. The plane wave is set to an energy of 600 eV. To model the surface of Bi and O doping in Bi solid solution, we use a (2×2) periodic slab models with four atomic layers combined with a 15 Å vacuum layer along the Z axis to eliminate the interaction between the slabs. The Brillouin zone integrations were performed using a 5×5×1 Monkhorst–Pack grid for (012) surfaces. In the slab calculations, the atoms in the bottom layer of the slab are fixed and other bottom atoms are allowed to relax. The atomic relaxation will be stop as soon as the energies within 1.0×10^{-5} eV/atom for total energy and the same the force on each atom is smaller than 0.01 eV/Å for force on every atom. The adsorption energies (E_{ads}) are calculated using following Equation:

$$E_{ads} = E_{ads} - (E_{slab} + E_{OH^-}) \quad (5)$$

where E_{ads}, E_{slab}, and E_{OH^-} correspond to the total energy of an adsorbate bound to the Bi or Bi with O doping (012) surface, a bare Bi or Bi with O doping (012) surface and an isolated OH^- group, respectively. By this definition, a negative value, corresponding to an exothermic process, indicates a stable adsorption.

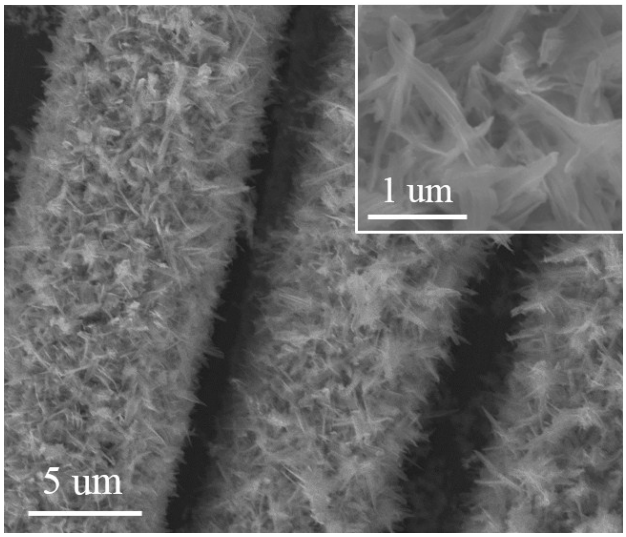

Fig. S1 SEM image of the pristine Bi sample.

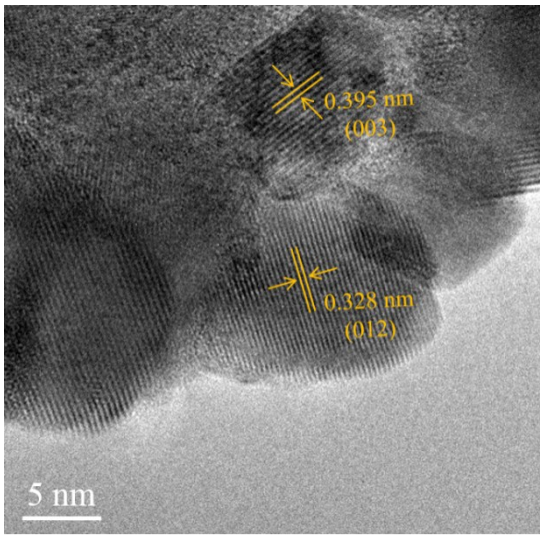

Fig. S2 TEM image of the pristine Bi sample.

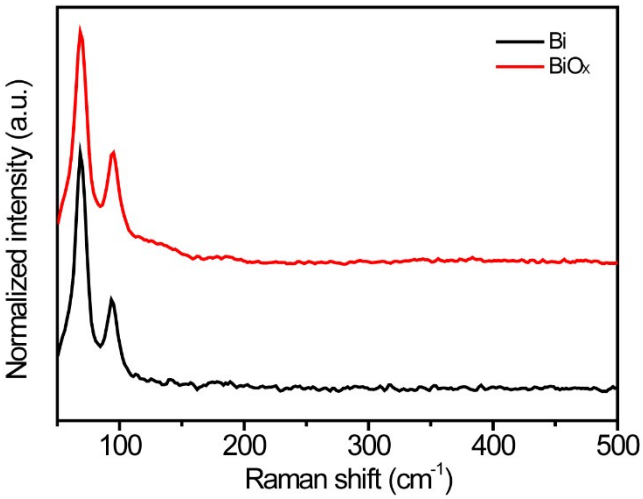

Fig. S3 Raman spectra of the pristine Bi and BiO_x electrodes.

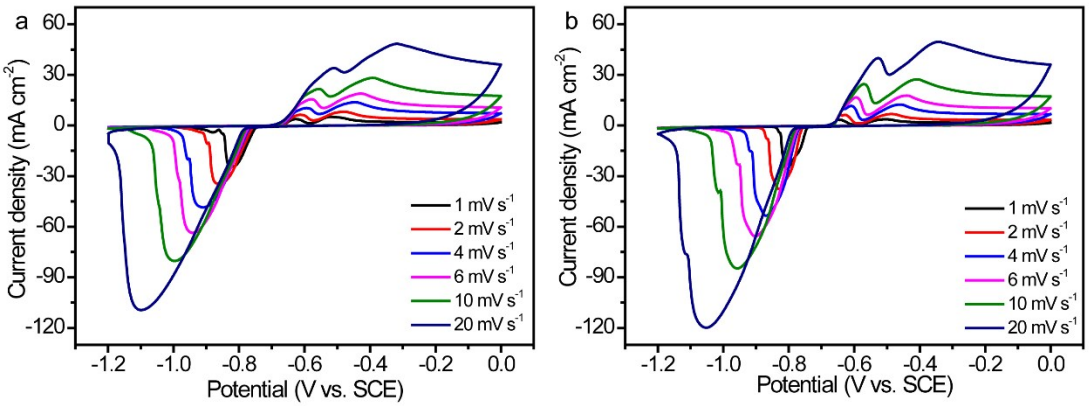

Fig. S4 CV cureves of the (a) pristine Bi and (b) BiO_x electrodes at various scan rates.

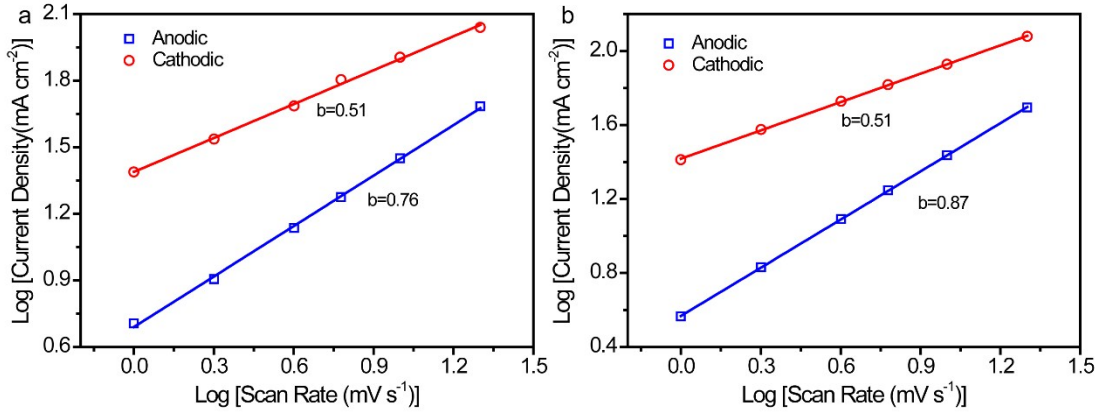

Fig. S5 Determination of the b-value using the relationship between anode and cathode peak currents and scan rates. (a) is pristine Bi and (b) is BiO_x electrodes.

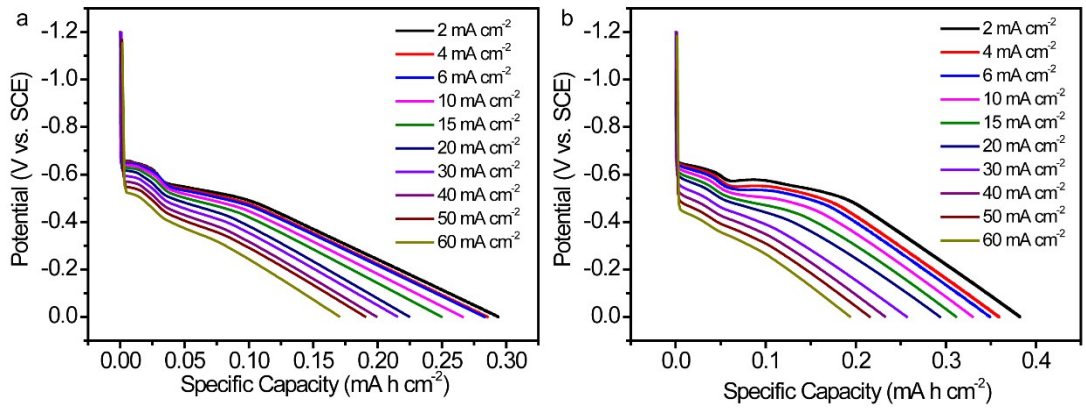

Fig. S6 Discharge curves of the (a) pristine Bi and (b) BiO_x electrodes at various current densities.

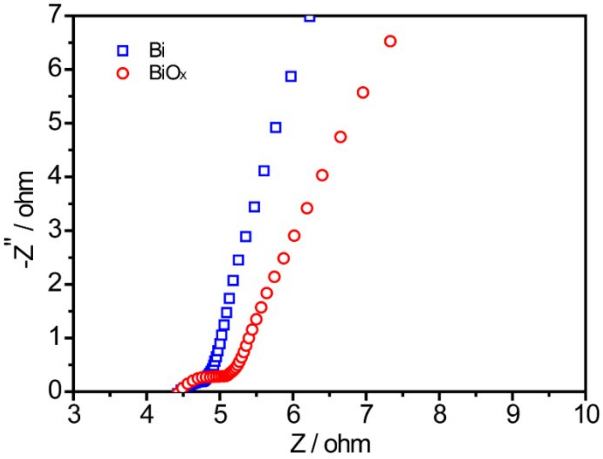

Fig. S7 Nyquist plots of the pristine Bi and BiO_x electrodes.

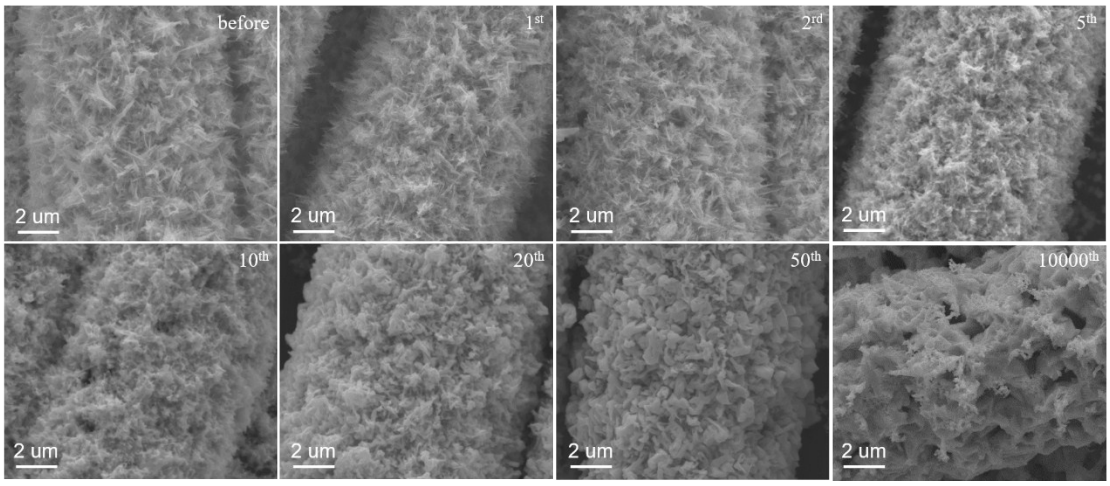

Fig. S8 SEM images of the pristine Bi electrode after certain cycles test.

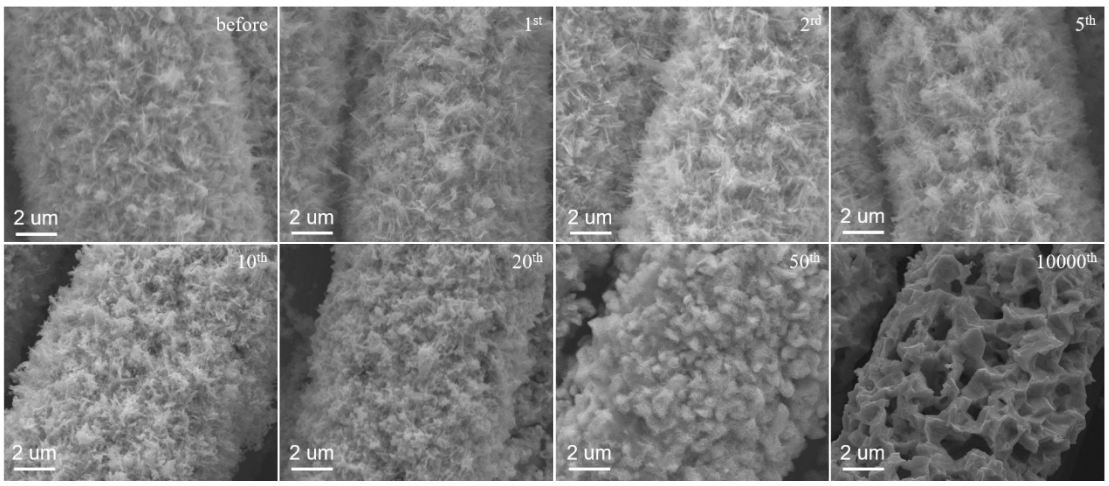

Fig. S9. SEM images of the BiO_x electrode after certain cycles test.

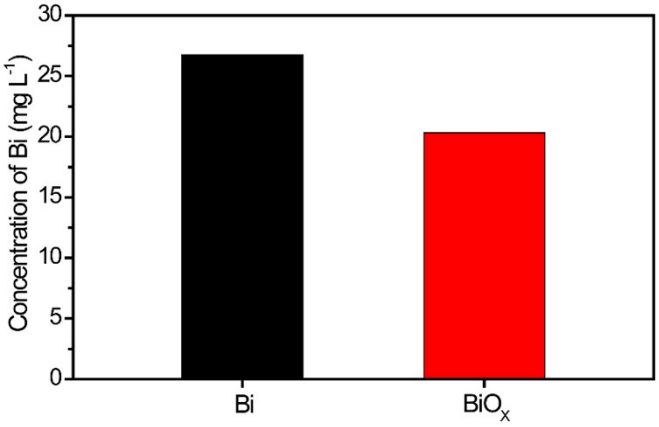

Fig. S10 Concentration of Bi in electrolyte for the pristine Bi and BiO_x electrodes after 20000 cycles test.

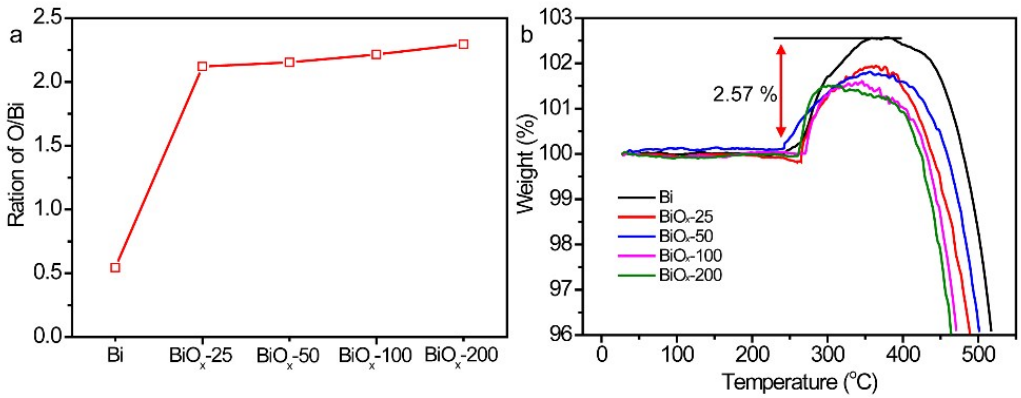

Fig. S11 (a) Ratio of O/Bi for the pristine Bi and BiO_x electrodes with different oxidation degree. (b) TGA results for the BiO_x electrodes with different oxidation degree.

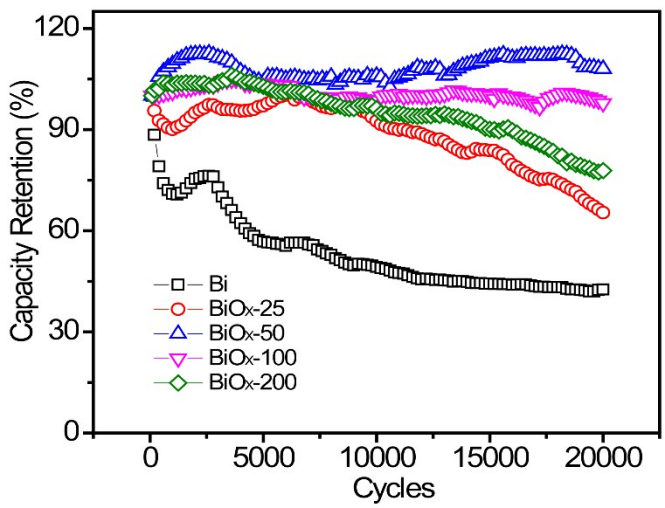

Fig. S12 Cycling performance of the pristine Bi and BiO_x electrodes with different oxidation degree for 20000 cycles tested at 100 mV s^{-1}.

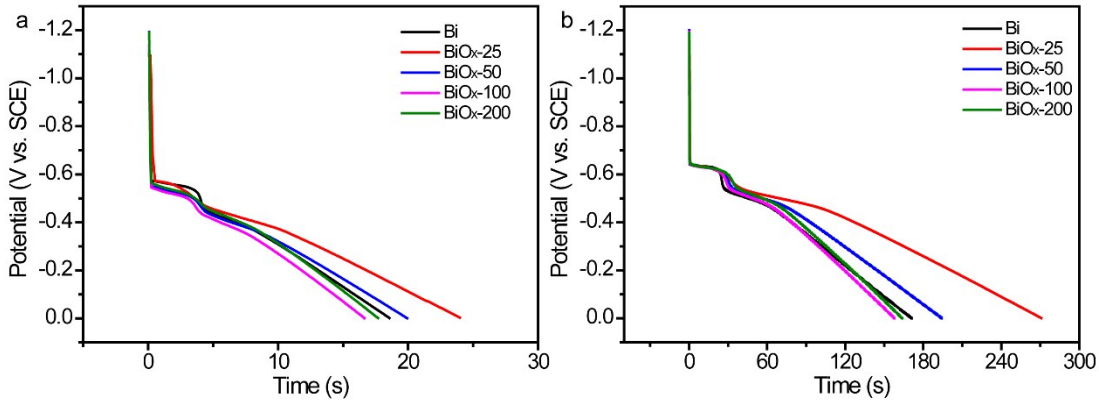

Fig. S13 Discharge curves of the pristine Bi and BiO_x electrodes with different oxidation degree at (a) 40 mA cm^{-2} and (b) 6 mA cm^{-2}.

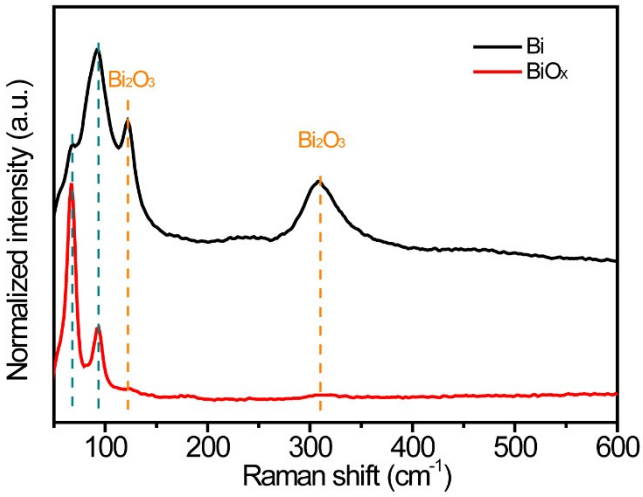

Fig. S14 Raman spectra of the pristine Bi and BiO_x electrodes after 20000 cycles test.

Table S1 The ratios of O/Bi for the pristine Bi and BiO_x electrodes after certain cycles.

	Initial	10	50	100	200	500	1000	5000	10000
Pristine Bi	0.23	0.59	0.74	0.89	0.95	1.02	1.07	1.14	1.21
BiO_x	0.52	0.54	0.53	0.55	0.55	0.56	0.58	0.63	0.69

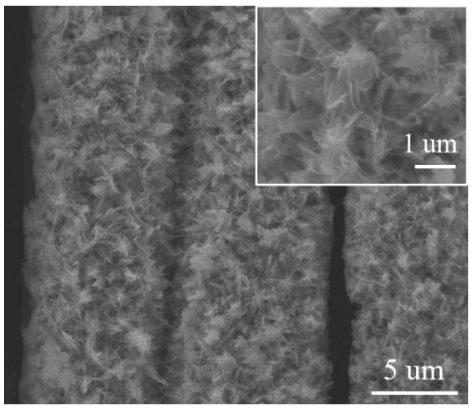

Fig. S15. SEM images of BiO_x electrode after ultrasounding for 1h.

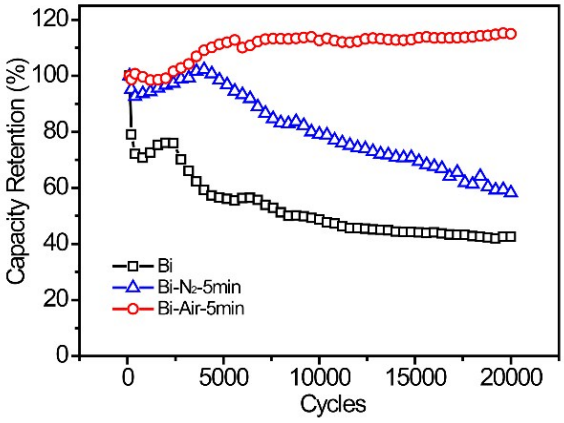

Fig. S16 Cycling performance of the Bi electrode annealed at 200 ^{o}C for 5 min in air tested at 100 mV s^{-1} for 20000 cycles.

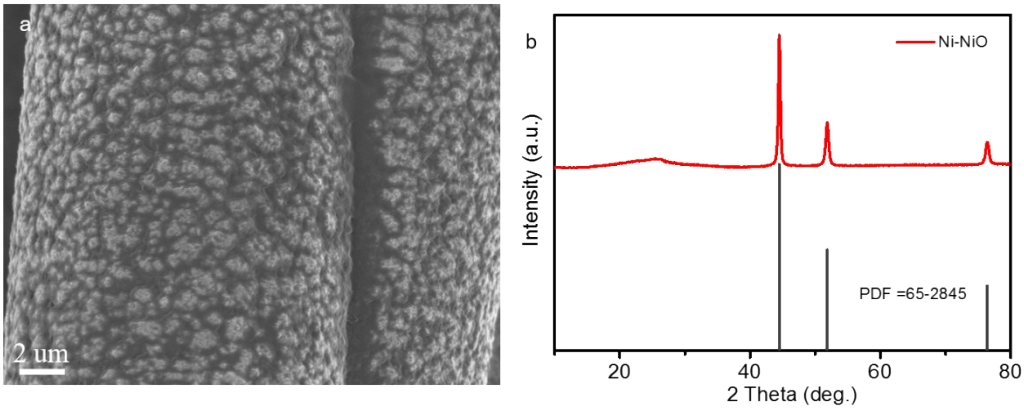

Fig. S17 (a) SEM image (b) XRD pattern of the as-preapred Ni-NiO electrode.

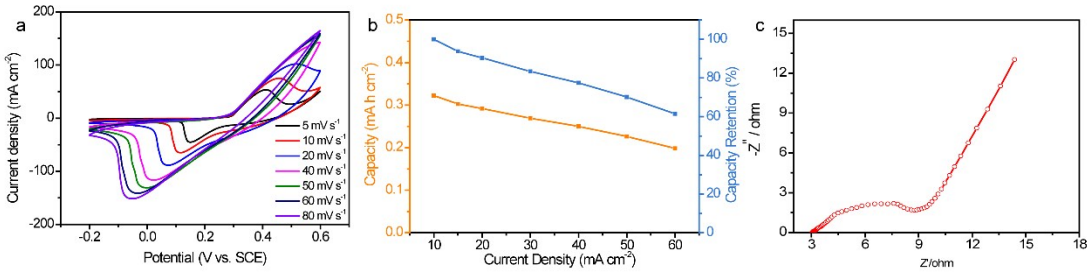

Fig. S18 (a) CV curves (b) Areal capacity and capacity retention as a function of current density obtained from discharge curves. (c) Nyquist plots of the Ni-NiO electrode.

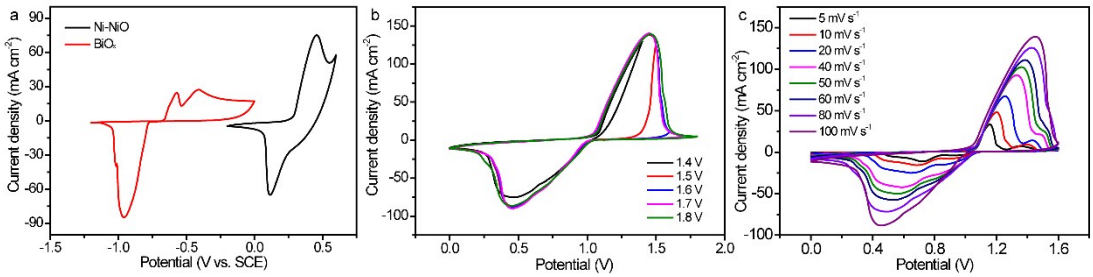

Fig. S19 (a) CV curves collected for Ni-NiO cathode and BiO_x anode at a scan rate of 40 mV s^{-1}. (b) CV curves collected for the Ni//Bi battery at various voltage windows at a scan rate of 100 mV s^{-1}. (c) CV curves collected for the Ni//Bi battery.

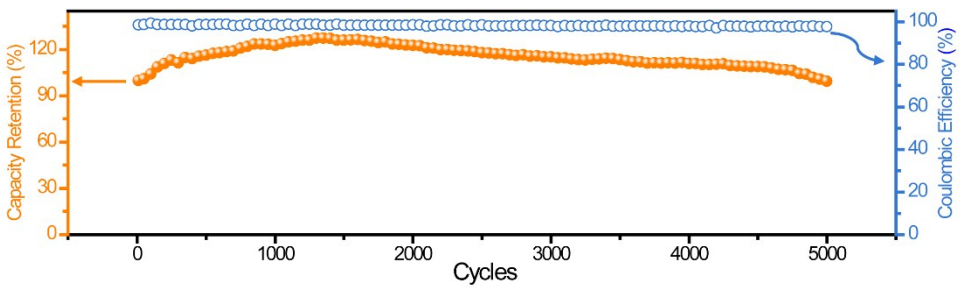

Fig. S20 Cycling performance and Coulombic efficiency of the Ni//Bi battery tested at 40 mA cm^{-2} for 5000 cycles.

Table S2 Comparison of the cycling performance of the Ni//Bi battery with recently reported aqueous rechargeable batteries.

Anode	Cathode	Cycling performance
BiO_x	Ni-NiO	96% after 5000 cycles (This work)
Bi	$NiCo_2O_4$	89% after 1000 cycles[1]
Bi/C	Ni-NiO	94% after 5000 cycles[2]
FeO_x/graphene	$Ni(OH)_2$/MWNT	~80% after 800 cycles[3]
CNTs/Fe_2O_3	CNTs/$Ni(OH)_2$	89.1% after 1000 cycles[4]
CC–CF@Fe_3O_4	CC–CF@NiO	70.5% after 2000 cycles[5]
Zn nanoflakes	nickel cobalt hydroxide	60% after 1000 cycles[6]
CC-CF@ZnO	CC-CF@NiO	72.9% after 2400 cycles[7]
Zn	P–$NiCo_2O_{4-x}$	73.8% after 5000 cycles[8]
Zn	Co-doped-$Ni(OH)_2$	88% after 5000 cycles[9]
Zn@CF	Co_3O_4	80% after 2000 cycles[10]
CC-ZnO@C-Zn	$Co(CO_3)_{0.5}(OH)_x \cdot 0.11H_2O$@$CoMoO_4$	71.1% after 5000 cycles[11]
Zn	Co(III) rich-Co_3O_4	92% after 5000 cycles[12]
Zn	$V_3O_7 \cdot H_2O$	60% after 200 cycles[13]
Zn	$Zn_3V_2O_7(OH)_2 \cdot 2H_2O$	68% after 300 cycles[14]
Zn	VO_2	91.2% after 300 cycles[15]
Zn	$V_2O_5 \cdot nH_2O$/graphene	71% after 900 cycles[16]
Zn	$Zn_{0.25}V_2O_5 \cdot nH_2O$	~80% after 1000 cycles[17]
Zn	$Na_2V_6O_{16} \cdot 3H_2O$	~80% after 1000 cycles[18]
Zn	$Na_{0.33}V_2O_5$	93% after 1000 cycles[19]
Zn	$Zn_2(OH)VO_4$	89% after 2000 cycles[20]
Zn	$Ca_{0.25}V_2O_5 \cdot nH_2O$	78% after 5000 cycles[21]
Zn	$ZnMn_2O_4$/C	94% after 500 cycles[22]
Zn	MnO_2	94% after 2000 cycles[23]
Zn	MnO_2	92% after 5000 cycles[24]

References：

1. Y. Zeng, Z. Lin, Y. Meng, Y. Wang, M. Yu, X. Lu and Y. Tong, *Adv. Mater.*, 2016, 28, 9188-9195.
2. Y. Zeng, Z. Lin, Z. Wang, M. Wu, Y. Tong and X. Lu, *Adv. Mater.*, 2018, 30, 1707290.
3. H. Wang, Y. Liang, M. Gong, Y. Li, W. Chang, T. Mefford, J. Zhou, J. Wang, T. Regier, F. Wei and H. Dai, *Nat. Commun.*, 2012, 3, 917.
4. J. Liu, M. Chen, L. Zhang, J. Jiang, J. Yan, Y. Huang, J. Lin, H. J. Fan and Z. X. Shen, *Nano Lett.*, 2014, 14, 7180-7187.
5. C. Guan, W. Zhao, Y. Hu, Q. Ke, X. Li, H. Zhang and J. Wang, *Adv. Energy Mater.*, 2016, 6, 1601034.
6. Y. Huang, W. S. Ip, Y. Y. Lau, J. Sun, J. Zeng, N. S. S. Yeung, W. S. Ng, H. Li, Z. Pei, Q. Xue, Y. Wang, J. Yu, H. Hu and C. Zhi, *ACS Nano*, 2017, 11, 8953-8961.

7. J. Liu, C. Guan, C. Zhou, Z. Fan, Q. Ke, G. Zhang, C. Liu and J. Wang, *Adv. Mater.*, 2016, 28, 8732-8739.
8. Y. Zeng, Z. Lai, Y. Han, H. Zhang, S. Xie and X. Lu, *Adv. Mater.*, 2018, 30, 1802396.
9. C. Xu, J. Liao, C. Yang, R. Wang, D. Wu, P. Zou, Z. Lin, B. Li, F. Kang and C.-P. Wong, *Nano Energy*, 2016, 30, 900-908.
10. X. Wang, F. Wang, L. Wang, M. Li, Y. Wang, B. Chen, Y. Zhu, L. Fu, L. Zha, L. Zhang, Y. Wu and W. Huang, *Adv. Mater.*, 2016, 28, 4904-4911.
11. M. Li, J. Meng, Q. Li, M. Huang, X. Liu, K. A. Owusu, Z. Liu and L. Mai, *Adv. Funct. Mater.*, 2018, 28, 1802016.
12. L. Ma, S. Chen, H. Li, Z. Ruan, Z. Tang, Z. Liu, Z. Wang, Y. Huang, Z. Pei, J. A. Zapien and C. Zhi, *Energy Environ. Sci.*, 2018, 11, 2521-2530.
13. D. Kundu, S. Hosseini Vajargah, L. Wan, B. Adams, D. Prendergast and L. F. Nazar, *Energy Environ. Sci.*, 2018, 11, 881-892.
14. C. Xia, J. Guo, Y. Lei, H. Liang, C. Zhao and H. N. Alshareef, *Adv. Mater.*, 2018, 30, 1705580.
15. J. Ding, Z. Du, L. Gu, B. Li, L. Wang, S. Wang, Y. Gong and S. Yang, *Adv. Mater.*, 2018, 30, e1800762.
16. M. Yan, P. He, Y. Chen, S. Wang, Q. Wei, K. Zhao, X. Xu, Q. An, Y. Shuang, Y. Shao, K. T. Mueller, L. Mai, J. Liu and J. Yang, *Adv. Mater.*, 2018, 30, 1703725.
17. D. Kundu, B. D. Adams, V. Duffort, S. H. Vajargah and L. F. Nazar, *Nature Energy*, 2016, 1, 16119.
18. V. Soundharrajan, B. Sambandam, S. Kim, M. H. Alfaruqi, D. Y. Putro, J. Jo, S. Kim, V. Mathew, Y.-K. Sun and J. Kim, *Nano Lett.*, 2018, 18, 2402-2410.
19. P. He, G. Zhang, X. Liao, M. Yan, X. Xu, Q. An, J. Liu and L. Mai, *Adv. Energy Mater.*, 2018, 8, 1702463.
20. D. Chao, C. R. Zhu, M. Song, P. Liang, X. Zhang, N. H. Tiep, H. Zhao, J. Wang, R. Wang, H. Zhang and H. J. Fan, *Adv. Mater.*, 2018, 30, e1803181.
21. C. Xia, J. Guo, P. Li, X. Zhang and H. N. Alshareef, *Angew. Chem. Int. Ed.*, 2018, 57, 3943-3948.
22. N. Zhang, F. Cheng, Y. Liu, Q. Zhao, K. Lei, C. Chen, X. Liu and J. Chen, *J. Am. Chem. Soc.*, 2016, 138, 12894-12901.
23. N. Zhang, F. Cheng, J. Liu, L. Wang, X. Long, X. Liu, F. Li and J. Chen, *Nat. Commun.*, 2017, 8, 405.
24. H. Pan, Y. Shao, P. Yan, Y. Cheng, K. S. Han, Z. Nie, C. Wang, J. Yang, X. Li, P. Bhattacharya, K. T. Mueller and J. Liu, *Nature Energy*, 2016, 1, 16039.